PROCEEDINGS OF SCIENCE

Surprises on the way to the QCD phase diagram

Owe Philipsen[a,b,*]

[a] *Institute for Theoretical Physics, Goethe University Frankfurt, Max-von-Laue-Str. 1, D-60438 Frankfurt am Main, Germany*

[b] *John von Neumann Institute for Computing (NIC) at GSI, Planckstr. 1, 64291 Darmstadt, Germany*

E-mail: philipsen@itp.uni-frankfurt.de

Lattice results over the last few years are reviewed, which have produced some unexpected insights into the QCD phase structure. The chiral phase transition in the limit of massless quarks is likely of second order for all $N_f = 2-6$, and remains second order independent of the value of an imaginary chemical potential for baryon number. On the other hand, for physical quark masses and zero density an approximate $SU(4)$ chiral spin symmetry is observed to emerge in a temperature range above the chiral crossover $T_{\rm ch}$, which reduces to the expected chiral symmetry at a second crossover $\sim 3T_{\rm ch}$. Spectral functions for pseudoscalar mesons, which successfully reproduce both spatial and temporal lattice correlators, show resonance-like peaks above the chiral crossover $T_{\rm ch}$, suggesting the presence of chirally symmetric, hadron-like thermoparticles in this regime. Implications for the QCD phase diagram are discussed.

European network for Particle physics, Lattice field theory and Extreme computing (EuroPLEx2023)
11-15 September 2023
Berlin, Germany

*Speaker

PoS(EuroPLEx2023)021

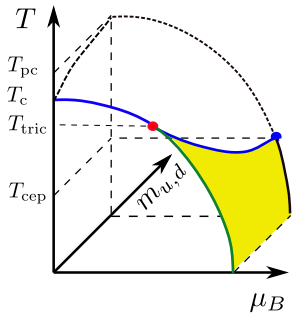

Figure 1: Connection of the putative QCD phase diagram for physical light quark masses to the chiral limit in the front plane.

1. Introduction

Due to the smallness of the u, d-quark masses, the physical QCD phase diagram should be closely related to the phase diagram in the chiral limit of $m_{u,d} = 0$. In the latter case the phase boundary as a function of temperature T and baryon chemical potential μ_B must represent a non-analytic phase transition. The commonly expected qualitative phase diagram in $(T, \mu_B, m_{u,d})$-space [1–4], connecting the chiral limit with the physical situation, is depicted in Fig. 1. It is mostly based on intuition from low energy effective models for QCD, like linear sigma models, the Namu-Jona-Lasinio model or quark-meson models, which typically predict the chiral transition to be of first order at vanishing temperature and of second order with $O(4)$ universality at zero density. This requires the existence of a tricritical point, where the transition switches order. From the tricritical point in the $m_{u,d} = 0$ symmetry plane emmanates a second-order wing line in the direction of the symmetry-breaking field, which for $m_{u,d} = m_{\rm phys}$ corresponds to the expected critical endpoint [4]. It must be stressed that these expectations were formulated using model input. Using symmetry arguments alone, the chiral transition in the massless limit could in principle also be entirely of first or second order, without changing its nature, with quite different implications for the physical point. These scenarios illustrate the importance of determining the QCD phase transition in the chiral limit from first principles, even at zero density.

2. The nature of the chiral transition

2.1 The Columbia plot at $\mu_B = 0$

The chiral phase transition in the limit of massless quarks cannot be simulated directly, even at zero density. For nearly 40 years intuition on the chiral phase transition was guided by the pioneering paper of Pisarski and Wilczek [5], who investigated the renormalisation group flow of a three-dimensional sigma-model, supplemented by a 't Hooft term for the $U(1)_A$ anomaly, as a finite temperature effective theory for the chiral condensate by means of the epsilon expansion. For $N_f \geq 3$ degenerate massless flavours, no stable fixed point was found which would imply the phase transition to be of first order. For $N_f = 2$ two different scenarios were proposed, with an $O(4)$ second-order transition in case the $U(1)_A$ remains anomalous at the chiral transition, and a first-order transition in case it gets effectively restored. Later, also a second-order option

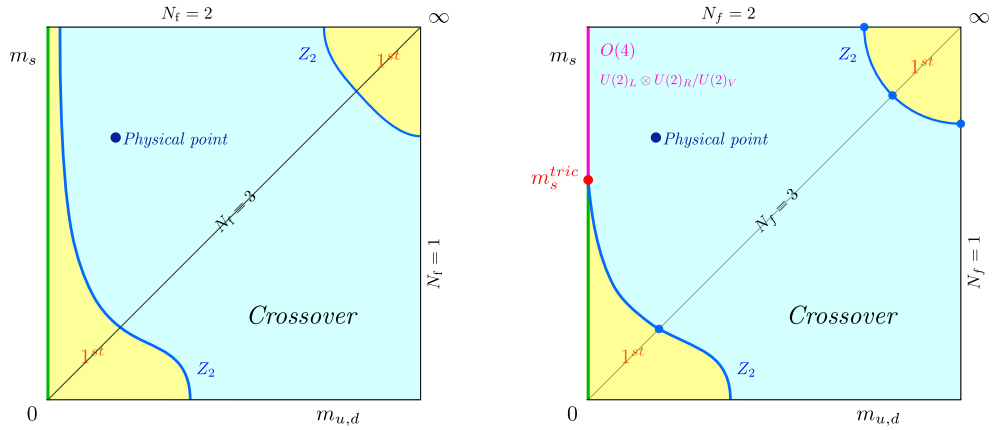

Figure 2: The order of the QCD thermal transition as a function of the quark masses. Possible scenarios proposed in [5] and observed on coarse lattices. From [6].

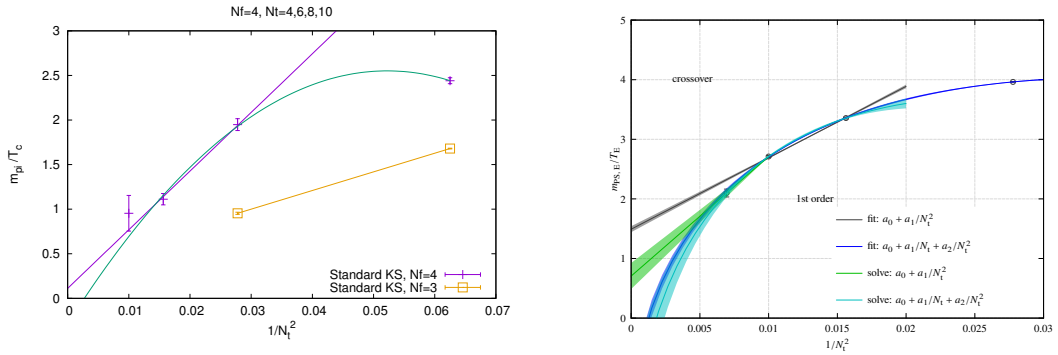

Figure 3: The pion mass evaluated on the critical boundary between the crossover and first-order regions. Left: $N_f = 3, 4$ unimproved staggered quarks [11]. Right: $O(a)$-improved Wilson quarks [12].

with a larger $U(2)_L \times U(2)_R/U(2)_V$ universality was suggested for this latter case [7]. Early lattice simulations [8, 9] were consistent with these possibilities, which are displayed in so-called Columbia plots, Fig. 2.

Distinguishing between these two scenarios by lattice simulations is a formidable task because of the necessity to take both a continuum and chiral limit in the appropriate order. Moreover, determining the location of the $Z(2)$-critical boundary line, which separates the mass ranges with crossover behaviour from the one with a first-order chiral transition, requires finite size scaling analyses of generalised cumulants of the order parameter over large portions of parameter space, and is significantly hampered by critical slowing down. The general observation over the last two decades is that this boundary is severely cutoff-dependent: it moves towards smaller quark masses, i.e. the first-order region shrinks drastically, as the lattice is made finer. Examples from the literature are shown in Fig. 3. Note that the first-order region on an $N_\tau = 6$ lattice is nearly twice as wide for $O(a)$-imrpoved Wilson fermions than it is for unimproved staggered fermions. On the other hand, improved staggered actions see no first-order region at all in the accessible light-mass range. For a more comprehensive review and reference list, see [10].

In order to resolve these issues, a new apporach was proposed in [13] by means of a change of

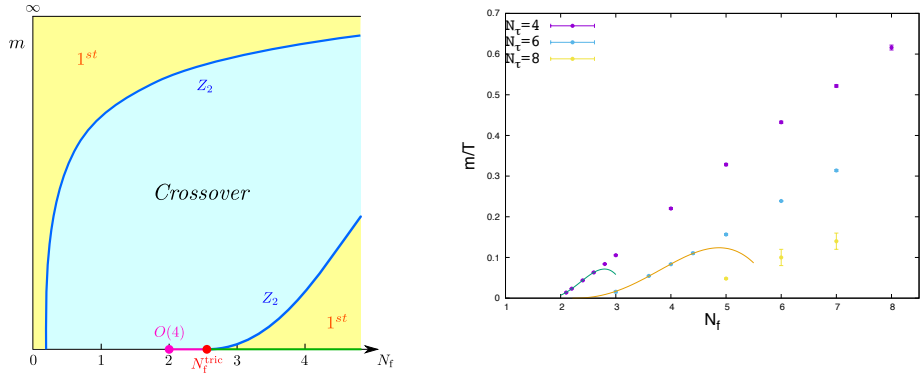

Figure 4: Left: Columbia plot for strictly degenerate quarks with a continous number of flavours N_f. Right: Data from simulations with standard staggered quarks for the critical line separating the crossover region (above) from the first-order region (below) [6].

variables. Instead of interpolating between $N_f = 3$ and $N_f = 2$ degenerate light quarks by varying $m < m_s < \infty$, one may also consider strictly degenerate quarks with mass m and, once the quarks have been integrated out (in continuum notation),

$$Z(N_f, g, m) = \int \mathcal{D}A \, (\det M[A; m])^{N_f} \, e^{-S_{\rm YM}[A]} \, , \tag{1}$$

the theory can be formally viewed as a statistical system of gauge field variables depending on a continuous parameter $2 < N_f < 3$. In particular for staggered fermions, whose determinant is raised to the power $N_f/4$ in order to describe N_f mass-degenerate quarks, this is implemented straightforwardly. The scenario Fig. 2 (right) then translates into Fig. 4 (left), with a tricritical $N_f^{\rm tric}$ replacing the tricritical strange quark mass of the original formulation. The $Z(2)$-critical wing line enters the tricritical point in the chiral limit as

$$N_f^c = N_f^{\rm tric} + A(am)^{2/5} + B(am)^{4/5} \, . \tag{2}$$

The mean field exponents in this expression are universal because the upper critical dimenison for tricriticality is three (for a review on tricriticality, see [14]). This formulation offers an advantage over the original one: since there is no chiral phase transition for $N_f \leq 1$, any first-order transition observed for $N_f \geq 3$ must necessarily disappear in a tricritical point as N_f is gradually reduced. Thus the same strategy can be applied independent of the final outcome: starting with a given $m_c(N_f \geq 3)$, follow the boundary line between the first-order and crossover region towards smaller N_f. Once tricritical scaling as in (2) can be established, an extrapolation to the lattice chiral limit is possible providing $N_f^{\rm tric}$. On the lattice, there is an additional dependence on the lattice spacing, viz. N_τ (with $T = (aN_\tau^{-1})$, so that there is a tricritical line $N_f^{\rm tric}(N_\tau)$ in the lattice bare parameter space. The scenario Fig. 2 (left) then corresponds to $N_f^{\rm tric} < 2$ in the continuum limit, and the scenario Fig. 2 (right) corresponds to $2 < N_f^{\rm tric} < 3$ in the continuum limit.

Fig. 4 (right) shows data obtained with unimproved staggered fermions for various N_f and three different $N_\tau = 4, 6, 8$ [6]. The realisation of the schematic plot on the left is obvious, with a first-order region below and crossover above the calculated critical lines. Indeed, good fits to (2)

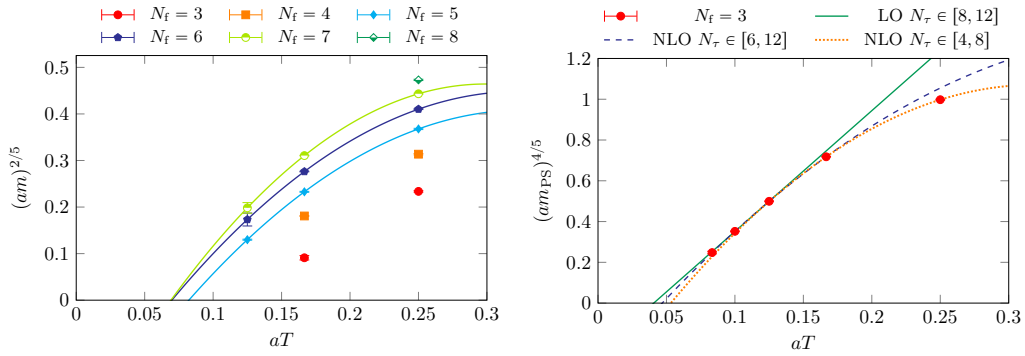

Figure 5: The $Z(2)$-critical line separating first-order transitions (below) from crossover (above), for unimproved staggered fermions [6] (left) and $O(a)$-improved Wilson fermions [12] (right), with tricritical scaling fits to both. From [6].

are possible, suggesting that tthe quark masses are sufficiently small to have attained the tricritical scaling region. From the extrapolation to the lattice chiral limit we learn that $N_f^{\rm tric}(N_\tau = 4) \approx 1.71(3)$ and $N_f^{\rm tric}(N_\tau = 6) \approx 2.20(8)$. Thus, on the coarsest $N_\tau = 4$ lattices the chiral transition looks as in Fig. 2 (left), whereas on $N_\tau = 6$ the scenario Fig. 2 (right) is realised. The $N_\tau = 8$ data show that there is no sign of the critical line converging towards a continuum limit, and no sign of the intercept $N_f^{\rm tric}(N_\tau)$ to approach a continuum limit either. In fact the data suggest the surprising conclusion that the confinuum limit $N_f^{\rm tric}(N_\tau = \infty) > 3$.

A powerful check on this is that indeed analogous scaling forms are observed to hold when the same data are projected to the (β, am) and (N_τ^{-1}, am) parameter planes instead [6]. The latter is shown in Fig. 5 (left). This plot is restricted to integer N_f values and just shows the behaviour of the critical quark mass delimiting the first-order region as a function of lattice spacing. Note however the rescaling of the vertical axis, so that (nearly) straight lines signal consistency with (NLO) tricritical scaling. The corresponding extrapolations to the lattice chiral limit now produce a function $N_\tau^{\rm tric}(N_f)$, the inversion of the one discussed in the previous paragraph. Note that the continuum limit is in the lower left corner of the plot. The existence of a finite $N_\tau^{\rm tric}(N_f)$ then implies that for this value of N_f any first-order chiral transition disappears once $N_\tau > N_\tau^{\rm tric}$. In other words, first-order regions terminating in a finite $N_\tau^{\rm tric}$ are not continously connected to the conitnuum limit and must be regarded as a lattice artefact. An important check of this statement is to test for the opposite behaviour. If the first-order region for a given N_f connects to the continuum limit, then there is no tricritical point and the critical quark mass in lattice units must go to zero as an ordinary polynomial

$$am_c(a) = \underbrace{am_c(0)}_{=0} + c_1(aT) + c_2(aT)^2 + \ldots \tag{3}$$

The data for $N_f = 5, 6, 7$ are incompatible with such behaviour, producing either $\chi^2_{\rm dof} > 10$ or negative mass ranges. Taking the uncertainty in the extrapolation into account, the analysis in this variable pairing then leads us to the even stronger conclusion that any tricritical point in the continuum is at $N_f^{\rm tric}(N_\tau = \infty) > 6$. Going back to our original case of interest, this implies that the $N_f = 3$ theory in the chiral limit has a second-order phase transition.

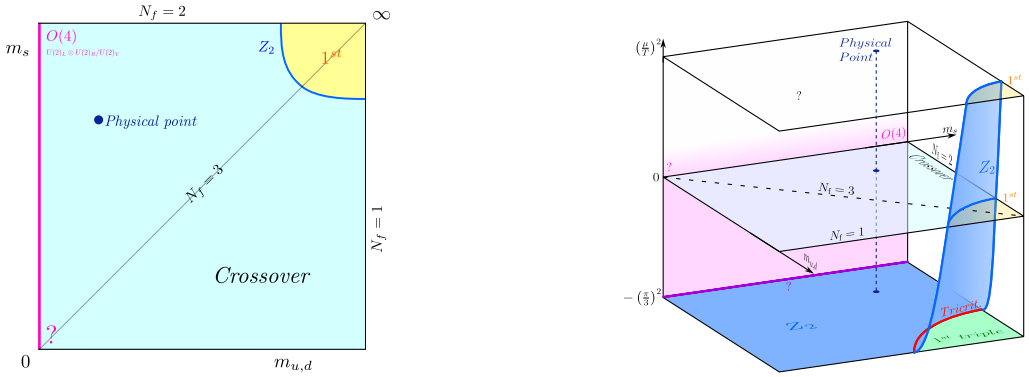

Figure 6: Leftt: Emerging continuum limit for the Columbia plot. The universality class in the three-flavour chiral limit is not yet known. From [6]. Right: Extension of the Columbia plot to non-vanishing quark chemical potentials, $\mu^2 \neq 0$. Negative μ^2 are fully accessible without sign problem.

An immediate question is whether this finding is stable under a change of lattice action. For the most interesting case of $N_f = 3$ we can immediately compare with the $O(a)$-improved Wilson data from Fig. 3 (right). Replotting the same data with a rescaled vertical axis, and taking into account that the pion mass $am_{PS}^2 \sim am$ towards the chiral limit, we obtain Fig. 5 (right). Perfect tricritical scaling is observed, with fits far better than the original polynomial ones. Hence, also $O(a)$-improved Wilson fermions are consistent with their first-order chiral transition terminating at a finite $N_\tau^{\rm tric}$, and therefore a second-order chiral transition in the continuum and chiral limits. In similar developments, no signal for any non-analytic phase transition in the $N_f = 3$ theory is observed using Highly Improved Staggered Quarks for pion masses down to $m_{PS} \approx 40$ MeV [15], as well as using domain wall fermions down to physical light quark mass values [16, 17]. The scenario with a second-order chiral transition at quark mass zero is therefore the only one without contradictions between different discretisations.

The emerging result for the Columbia plot in the continuum is shown in Fig. 6 (left), with a second-order phase transition at $m_{u,d} = 0$ for *all* strange quark masses. Note that the universality class presumably changes between the $N_f = 2, 3$ limits, where the effective chiral symmetry in the lower left corner again depends on the fate of the axial anomaly. Finally, renewed investigations of the most general low energy scalar models with fRG methods [18, 19] and numerical conformal bootstrap [20], as well as a QCD investigation based on Dyson-Schwinger equations [21] are all consistent with this picture, under certain conditions on the axial anomaly and related operators [22].

2.2 Extension to $\mu_B \neq 0$

The next question is how the Columbia plot changes when a baryon chemical potential is switched on. We restrict ourselves to purely imaginary chemical potentials, for which there is no sign problem. An ongoing project repeats the previous analysis of the N_f and N_τ-dependence of the chiral transition for unimproved staggered quarks at a fixed value of $\mu_B = i0.81\pi T$. Preliminary results show the same picture as at $\mu_B = 0$, i.e., all first-order transitions observed for $N_f \in [3, 6]$ disappear in tricritical points before the continuum is reached [23]. Consistent with this is the absence of any non-analytic chiral transition down to $m_{PS} \approx 50$ MeV in the Roberge-Weiss plane

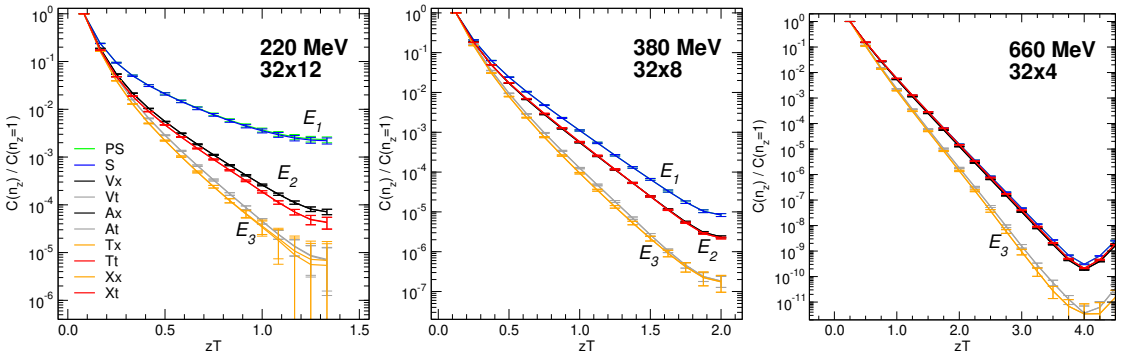

Figure 7: Spatial correlation functions with domain wall fermions show distinct E_1, E_2, E_3 multiplets of the approximate $SU(4)$ chiral spin symmetry, at temperatures above the crossover. At large temperatures, these reduce to the multiplets of the ordinary chiral symmetry. From [26].

at $\mu_B = i\pi T$, observed using stout-smeared staggered as well as HISQ simulations [24, 25]. An analysis of carefully truncated Dyson-Schwinger equations also finds a second-order transition at $m_{u,d} = 0$, which is stable under variations of chemical potential, both real and imaginary within $|\mu_B| < 30$ MeV. Altogether the Columbia plot can be extended by a μ^2-axis and looks like Fig. 6 (right). Based on all available lattice results, the nature of the chiral transition does not show any μ_B-dependence, at least in the imaginary direction. The widely expected phase diagram Fig. 1 would now require an additional critical surface branching off non-analytically from a tricritical line in the $(m_{u,d} = 0)$-plane at some $\mu_B > 0$.

3. Emergent chiral spin symmetry above the chiral crossover

A $SU(2)_{CS}$ chiral spin transformation of Dirac fields is defined as

$$\psi(x) \to \exp\left(i\vec{\Sigma}\cdot\vec{\epsilon}\right)\psi(x)\,, \quad \vec{\Sigma} = (\gamma_k, -i\gamma_5\gamma_k, \gamma_5)\,, \quad [\Sigma_i, \Sigma_j] = 2i\epsilon_{ijk}\Sigma_k\,, \tag{4}$$

with $k = 0, \ldots 3$ any of the euclidean gamma matrices. It is obvious that $SU(2)_{CS} \supset U(1)_A$. When combined with isospin, $SU(2)_{CS} \otimes SU(2)_V$ can be embedded into the larger $SU(4)$, which contains the full chiral symmetry of the massless QCD Lagrangian, $SU(4) \supset SU(2)_L \times SU(2)_R \times U(1)_A$. In presence of a thermal medium there is a preferred Lorentz frame, and the massless quark action can be written as

$$\bar{\psi}\gamma_\mu D_\mu\psi = \bar{\psi}\gamma_0 D_0\psi + \bar{\psi}\gamma_i D_i\psi\,, \quad \text{with} \quad [\Sigma_i, \gamma_0\gamma_0] = 0\,, \;\; [\Sigma_i, \gamma_0\gamma_j] \neq 0\,. \tag{5}$$

The colour-electric part of the quark-gluon interaction is thus CS- and $SU(4)$-invariant, while kinetic terms, and thus the free Dirac action, as well as colour-magnetic interactions are not. Therefore, chiral spin symmetry is never exact in physical QCD, but its approximate realisation is possible if the colour-electric quark-gluon interaction dominates the quantum effective action in some dynamical range. Surprisingly, this has been established to be realised in a temperature window of very roughly $T_{\rm ch} \lesssim T \lesssim 3T_{\rm ch}$, with $T_{\rm ch}$ denoting the chiral crossover temperature.

On the lattice one can test for symmetries by computing correlation functions and their assocuated degeneracy patterns. Consider the euclidean meson correlators with $J = 0, 1$ and Γ some Dirac matrix,

$$C_\Gamma(\tau, \mathbf{x}) = \langle O_\Gamma(\tau, \mathbf{x})\, O_\Gamma^\dagger(0, \mathbf{0})\rangle\,. \tag{6}$$

Full information about all excitations is contained in the associated spectral functions $\rho_\Gamma(\omega, \mathbf{p})$,

$$C_\Gamma(\tau, \mathbf{p}) = \int_0^\infty \frac{d\omega}{2\pi} K(\tau, \omega)\rho_\Gamma(\omega, \mathbf{p}) , \quad K(\tau, \omega) = \frac{\cosh(\omega(\tau - 1/2T))}{\sinh(\omega/2T)} . \tag{7}$$

In an isotropic system in equilibrium, the spectral function is sufficiently constrained by the spatial and temporal correlators averaged over the orthogonal directions,

$$C^s_\Gamma(z) = \sum_{x,y,\tau} C_\Gamma(\tau, \mathbf{x}) , \quad C^\tau_\Gamma(\tau) = \sum_{x,y,z} C_\Gamma(\tau, \mathbf{x}) . \tag{8}$$

An approximate multiplet structure compatible with the larger $SU(4)$ chiral spin symmetry has been observed in spatial [26] and temporal [27] correlators for $N_f = 2$ QCD with domain wall fermions, see examples in Fig. 7. While the multiplets E_1, E_3 are also there in the case of the ecpected chiral symmetry, the separate E_2 multiplet requires the larger $SU(4)$ synmetry. One is led to conclude that the colour-electric quark gluon interaction, which is responsible for the confining string in mesons, dynamically dominates this intermediate regime above the chiral crossover, and then gets screened at some higher temperature $T_s \sim 3T_{\rm ch}$, where the additional multiplet structure reduces to the expected chirally symmetric one. Such patterns have been confirmed in similar investigations using domain wall fermions with $N_f = 2 + 1$ [28] and $N_f = 2 + 1 + 1$ [29] flavours of quarks with physical masses. One would then conclude that the intermediate regime is chirally symmetric, but its dynamics still hadron-like rather than parton-like.

4. Pseudoscalar spectral function

Information about the nature of the effective degrees of freedom is contained in the spectral functions, Eq. (7), whose extraction from discrete sets of lattice correlator data represents an ill-posed inversion problem. However, the obstacle can be cicrumvented for stable, massive scalar particles, such as the pion in QCD. The approach is based on exploiting micro-causality, which ensures a representation of the spectral function [30, 31] in the form

$$\rho_{\rm PS}(\omega, \mathbf{p}) = \int_0^\infty ds \int \frac{d^3u}{(2\pi)^2} \epsilon(p_0)\, \delta\Big(\omega^2 - (\mathbf{p} - \mathbf{u})^2 - s\Big)\, \widetilde{D}_\beta(\mathbf{u}, s) , \tag{9}$$

with $\beta = 1/T$, and a thermal spectral density $\widetilde{D}_\beta(\mathbf{u}, s)$. This allows to recover the Källen-Lehmann vacuum representation smoothly as $T \to 0$. For stable massive particles, such as QCD pions, the authors argue for the analytic vacuum structure of the spectral density to be preserved in the absence of a true phase transition, and propose an ansatz with thermally modified particle (thermoparticle) and continuous scattering contributions,

$$\widetilde{D}_\beta(\mathbf{u}, s) = \widetilde{D}_{m,\beta}(\mathbf{u})\, \delta(s - m^2) + \widetilde{D}_{c,\beta}(\mathbf{u}, s) . \tag{10}$$

In an isotropic medium the spatial correlators and the spectral density are then related by [32]

$$C^s_{PS}(z) = \frac{1}{2} \int_0^\infty ds \int_{|z|}^\infty dR\, e^{-R\sqrt{s}} D_\beta(R, s). \tag{11}$$

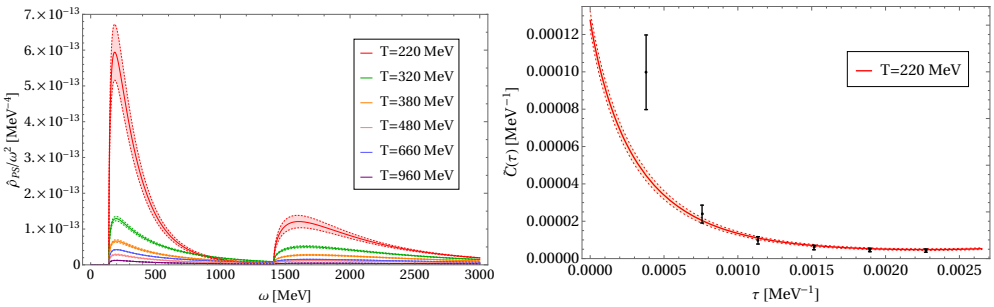

Figure 8: Left: Pion spectral function extracted from spatial lattice correlators. Right: Temporal correlator predicted by that spectral function, compared to lattice data. From [32].

For temperatures below the threshold to the scattering states one expects the first term in Eq. (10) to dominate. Neglecting the continuum part, the calculation of the spectral function is straightforward. First, the spatial pseudo-scalar correlators from Fig. 7 are fitted by the sum of two exponentials representing the π, π^*, which gives an excellent description of the data in the entire temperature range. This provides the $D_{m,\beta}(|\mathbf{x}|) = \alpha_{\pi,\pi^*} \exp(-\gamma_{\pi,\pi^*}|\mathbf{x}|)$, from which the spectral function can be reconstructed using Eqs. (9,10) and the vacuum masses m_π, m_{π^*},

$$\rho_{\rm PS}(\omega, \mathbf{p}=0) = \epsilon(\omega) \left[\theta(\omega^2 - m_\pi^2) \frac{4\,\alpha_\pi\,\gamma_\pi \sqrt{\omega^2 - m_\pi^2}}{(\omega^2 - m_\pi^2 + \gamma_\pi^2)^2} + \theta(\omega^2 - m_{\pi^*}^2) \frac{4\,\alpha_{\pi^*}\,\gamma_{\pi^*} \sqrt{\omega^2 - m_{\pi^*}^2}}{(\omega^2 - m_{\pi^*}^2 + \gamma_{\pi^*}^2)^2} \right]. \tag{12}$$

The result is shown in Fig. 8 (left) and displays the vacuum thresholds followed by a pronounced resonance-like peak structure for both the pion and its first excitation. As a non-trivial test, the temporal correlator is computed from the spectral function and compared to lattice data in Fig. 8 (right). A quantitatively accurate description is achieved except for the data point at the shortest distance, which is smaller than $m_{\pi^*}^{-1}$ and thus would require knowledge of higher excited states from the spatial correlator. As the temperature increases, the peaks widen and gradually disappear into a continuum, but only at temperatures significantly above $T_{\rm pc}$. This is in accord with the approximately chiral-spin symmetric window consisting of non-perturbative, hadron-like excitations. Finally, as a further test of the generality of the thermoparticle approach for moderate temperatures of the order of particle masses, equally successful descriptions are achieved for the QCD pseudoscalars involving strange quarks [33] as well as for the dynamically completely different ϕ^4-theory [34].

5. Implications for the QCD phase diagram

If there is an approximately chiral-spin symmetric temperature regime at zero density, then it must necessarily extend to $\mu_B \neq 0$, because baryon number $\sim \bar\psi\gamma^0\psi$ is invariant under chiral spin transformations. From the behaviour of screening masses with imaginary chemical potential one can infer that, for small chemical potentials, the chiral-spin symmetric band must bend downwards to lower temperatures [35]. As the baryon chemical potential increases, $\mu_B \gtrsim T$, no further lattice information is available and the further shape of this band is up to speculation. However, based

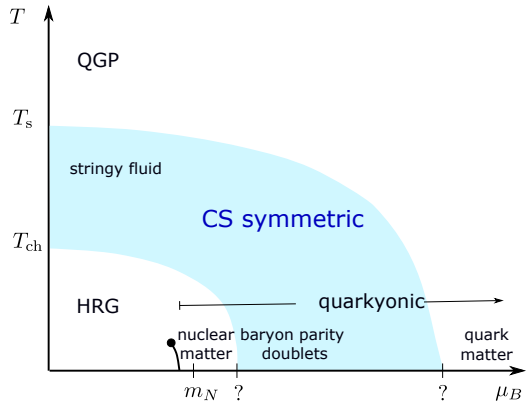

Figure 9: A possible QCD phase diagram with a chiral-spin symmetric band. From [35].

on large N_c arguments, a so-called quarkyonic regime has been postulated in the cold and dense regime beyond the baryon onset, in which the pressure scales as $p \sim N_c$ and which contains chirally symmetric baryon matter [36]. Indeed, such a pressure scaling could be established within an effective lattice theory derived by a combined character and hopping expansion [37]. Furthermore, baryon parity doublet models are not only chirally symmetric, but also chiral-spin symmetric [38]. Finally, for large N_c also the chiral-spin symmetric range in the temperature direction should show $p \sim N_c$ [39]. One plausible option would then be for these chirally symmetric and hadronic regions in the T- and μ_B-directions to be part of the same chiral-spin symmetric band, as sketched in Fig. 9. In addition, there may be a chiral phase transition line with a critical endpoint, such as predicted by functional renormalisation group [40, 41] and Dyson-Schwinger methods [42].

Acknowledgments: The author acknowledges support by the Deutsche Forschungsgemeinschaft (DFG) through the grant CRC-TR 211 "Strong-interaction matter under extreme conditions" and by the State of Hesse within the Research Cluster ELEMENTS (Project ID 500/10.006).

References

[1] A.M. Halasz, A.D. Jackson, R.E. Shrock, M.A. Stephanov and J.J.M. Verbaarschot, *On the phase diagram of QCD*, *Phys. Rev. D* **58** (1998) 096007 [hep-ph/9804290].

[2] M.A. Stephanov, K. Rajagopal and E.V. Shuryak, *Signatures of the tricritical point in QCD*, *Phys. Rev. Lett.* **81** (1998) 4816 [hep-ph/9806219].

[3] K. Rajagopal and F. Wilczek, *The Condensed matter physics of QCD*, in *At the frontier of particle physics. Handbook of QCD. Vol. 1-3*, M. Shifman and B. Ioffe, eds., pp. 2061–2151 (2000), DOI [hep-ph/0011333].

[4] Y. Hatta and T. Ikeda, *Universality, the QCD critical / tricritical point and the quark number susceptibility*, *Phys. Rev. D* **67** (2003) 014028 [hep-ph/0210284].

[5] R.D. Pisarski and F. Wilczek, *Remarks on the Chiral Phase Transition in Chromodynamics*, *Phys. Rev. D* **29** (1984) 338.

[6] F. Cuteri, O. Philipsen and A. Sciarra, *On the order of the QCD chiral phase transition for different numbers of quark flavours*, *JHEP* **11** (2021) 141 [2107.12739].

[7] A. Pelissetto and E. Vicari, *Relevance of the axial anomaly at the finite-temperature chiral transition in QCD*, *Phys. Rev. D* **88** (2013) 105018 [1309.5446].

[8] F.R. Brown, F.P. Butler, H. Chen, N.H. Christ, Z.-h. Dong, W. Schaffer et al., *On the existence of a phase transition for QCD with three light quarks*, *Phys. Rev. Lett.* **65** (1990) 2491.

[9] Y. Iwasaki, K. Kanaya, S. Kaya, S. Sakai and T. Yoshie, *Finite temperature transitions in lattice QCD with Wilson quarks: Chiral transitions and the influence of the strange quark*, *Phys. Rev. D* **54** (1996) 7010 [hep-lat/9605030].

[10] O. Philipsen, *Lattice Constraints on the QCD Chiral Phase Transition at Finite Temperature and Baryon Density*, *Symmetry* **13** (2021) 2079 [2111.03590].

[11] P. de Forcrand and M. D'Elia, *Continuum limit and universality of the Columbia plot*, *PoS* **LATTICE2016** (2017) 081 [1702.00330].

[12] Y. Kuramashi, Y. Nakamura, H. Ohno and S. Takeda, *Nature of the phase transition for finite temperature $N_{\rm f} = 3$ QCD with nonperturbatively O(a) improved Wilson fermions at $N_{\rm t} = 12$*, *Phys. Rev. D* **101** (2020) 054509 [2001.04398].

[13] F. Cuteri, O. Philipsen and A. Sciarra, *QCD chiral phase transition from noninteger numbers of flavors*, *Phys. Rev. D* **97** (2018) 114511 [1711.05658].

[14] I. Lawrie and S. Sarbach, *Theory of tricritical points*, in *Phase transitions and critical phenomena*, C. Domb and J. Lebowitz, eds., vol. 9, p. 1 (1984).

[15] L. Dini, P. Hegde, F. Karsch, A. Lahiri, C. Schmidt and S. Sharma, *Chiral phase transition in three-flavor QCD from lattice QCD*, *Phys. Rev. D* **105** (2022) 034510 [2111.12599].

[16] Y. Zhang, Y. Aoki, S. Hashimoto, I. Kanamori, T. Kaneko and Y. Nakamura, *Finite temperature QCD phase transition with 3 flavors of Mobius domain wall fermions*, *PoS* **LATTICE2022** (2023) 197 [2212.10021].

[17] Y. Zhang, Y. Aoki, S. Hashimoto, I. Kanamori, T. Kaneko and Y. Nakamura, *Exploring the QCD phase diagram with three flavors of Möbius domain wall fermions*, *PoS* **LATTICE2023** (2024) 203 [2401.05066].

[18] G. Fejos, *Second-order chiral phase transition in three-flavor quantum chromodynamics?*, *Phys. Rev. D* **105** (2022) L071506 [2201.07909].

[19] G. Fejos and T. Hatsuda, *Order of the SU(N_f) x SU(N_f) chiral transition via the functional renormalization group*, 2404.00554.

[20] S.R. Kousvos and A. Stergiou, *CFTs with $U(m) \times U(n)$ Global Symmetry in 3D and the Chiral Phase Transition of QCD*, 2209.02837.

[21] J. Bernhardt and C.S. Fischer, *QCD phase transitions in the light quark chiral limit*, *Phys. Rev. D* **108** (2023) 114018 [2309.06737].

[22] R.D. Pisarski and F. Rennecke, *The chiral phase transition and the axial anomaly*, 2401.06130.

[23] A. D'Ambrosio, O. Philipsen and R. Kaiser, *The chiral phase transition at non-zero imaginary baryon chemical potential for different numbers of quark flavours*, *PoS* **LATTICE2022** (2023) 172 [2212.03655].

[24] C. Bonati, E. Calore, M. D'Elia, M. Mesiti, F. Negro, F. Sanfilippo et al., *Roberge-Weiss endpoint and chiral symmetry restoration in $N_f = 2 + 1$ QCD*, *Phys. Rev. D* **99** (2019) 014502 [1807.02106].

[25] F. Cuteri, J. Goswami, F. Karsch, A. Lahiri, M. Neumann, O. Philipsen et al., *Toward the chiral phase transition in the Roberge-Weiss plane*, *Phys. Rev. D* **106** (2022) 014510 [2205.12707].

[26] C. Rohrhofer, Y. Aoki, G. Cossu, H. Fukaya, C. Gattringer, L.Y. Glozman et al., *Symmetries of spatial meson correlators in high temperature QCD*, *Phys. Rev. D* **100** (2019) 014502 [1902.03191].

[27] C. Rohrhofer, Y. Aoki, L.Y. Glozman and S. Hashimoto, *Chiral-spin symmetry of the meson spectral function above T_c*, *Phys. Lett. B* **802** (2020) 135245 [1909.00927].

[28] T.-W. Chiu, *Symmetries of meson correlators in high-temperature QCD with physical (u/d,s,c) domain-wall quarks*, *Phys. Rev. D* **107** (2023) 114501 [2302.06073].

[29] T.-W. Chiu, *Symmetries of spatial correlators of light and heavy mesons in high temperature lattice QCD*, 2404.15932.

[30] J. Bros and D. Buchholz, *Towards a relativistic KMS condition*, *Nucl. Phys. B* **429** (1994) 291 [hep-th/9807099].

[31] J. Bros and D. Buchholz, *Axiomatic analyticity properties and representations of particles in thermal quantum field theory*, *Ann. Inst. H. Poincare Phys. Theor.* **64** (1996) 495 [hep-th/9606046].

[32] P. Lowdon and O. Philipsen, *Pion spectral properties above the chiral crossover of QCD*, *JHEP* **10** (2022) 161 [2207.14718].

[33] D. Bala, O. Kaczmarek, P. Lowdon, O. Philipsen and T. Ueding, *Pseudo-scalar meson spectral properties in the chiral crossover region of QCD*, 2310.13476.

[34] P. Lowdon and O. Philipsen, *On the (in)consistency of perturbation theory at finite temperature*, 2405.02009.

[35] L.Y. Glozman, O. Philipsen and R.D. Pisarski, *Chiral spin symmetry and the QCD phase diagram*, *Eur. Phys. J. A* **58** (2022) 247 [2204.05083].

[36] L. McLerran and R.D. Pisarski, *Phases of cold, dense quarks at large N(c)*, *Nucl. Phys. A* **796** (2007) 83 [0706.2191].

[37] O. Philipsen and J. Scheunert, *QCD in the heavy dense regime for general N_c: on the existence of quarkyonic matter*, *JHEP* **11** (2019) 022 [1908.03136].

[38] M. Catillo and L.Y. Glozman, *Baryon parity doublets and chiral spin symmetry*, *Phys. Rev. D* **98** (2018) 014030 [1804.07171].

[39] T.D. Cohen and L.Y. Glozman, *Large N_c QCD phase diagram at $\mu_B = 0$*, 2311.07333.

[40] F. Gao and J.M. Pawlowski, *Chiral phase structure and critical end point in QCD*, *Phys. Lett. B* **820** (2021) 136584 [2010.13705].

[41] W.-j. Fu, J.M. Pawlowski and F. Rennecke, *QCD phase structure at finite temperature and density*, *Phys. Rev. D* **101** (2020) 054032 [1909.02991].

[42] C.S. Fischer, *QCD at finite temperature and chemical potential from Dyson–Schwinger equations*, *Prog. Part. Nucl. Phys.* **105** (2019) 1 [1810.12938].